AIAA 81-0018R

Disturbance Estimation for a STOL Transport During Landing

J.A. Bossi*
University of Washington, Seattle, Wash.
and
A.E. Bryson Jr.†
Stanford University, Stanford, Calif.

Transport aircraft can experience dangerously high sink rates if wind shear or thrust loss are encountered during landing approach. This is of special concern for STOL aircraft that use engine thrust for life augmentation. Such conditions must be detected quickly, and available power increased promptly to avoid serious flight path deviations. This study demonstrates the feasibility of designing constant-gain estimators, which use onboard instrumentation, to detect such conditions with sufficient speed and accuracy to provide adequate warning. Estimator design techniques are discussed and simulation results presented.

Nomenclature

A_{ac}, A_d = system dynamics matrices
a_h, a_v = horizontal and vertical wind rates
a_x, a_z = body-axis specific force measurements
B = control distribution matrix
C_{ac}, C_d = measurement distribution matrices
c_t = thrust coefficient ($\%T_{max}$)
c_{tc}, c_{td} = thrust inputs, command and disturbance
D = disturbance coupling matrix
$\dot{h}$ = altitude rate
K_{ac}, K_d = estimator gain matrices
L_h, L_v = horizontal and vertical turbulence scale length
q = pitch rate
R_i = measurement noise density
$\dot{r}$ = ground speed
s = Laplace variable (frequency)
T_{max} = maximum thrust force
u = x-axis inertial velocity
u = control input vector
u_a = airspeed
v_{wh}, v_{wv} = horizontal and vertical wind speed
w = z-axis inertial velocity
x_{ac} = aircraft state vector
x_d = disturbance state vector
z = measurement vector
α = age-weighting (or frequency shift) parameter
α_a = aerodynamic angle-of-attack
δ_e, δ_f = elevator and flap inputs
η = process noise vector
θ = pitch angle
ν = measurement noise vector
σ_n, σ_v = horizontal and vertical turbulence rms values
σ_i = measurement rms values
τ_m = measurement correlation time
$(\hat{\ })$ = estimate of a variable
$(\dot{\ })$ = time derivative of a variable

Introduction

WIND shear (i.e., change of wind speed with altitude or with time) can produce serious flight path deviations, and a number of transport aircraft accidents have been attributed to this cause.[1] Short Take-Off and Landing (STOL) aircraft, which use engine thrust for lift augmentation, are also highly sensitive to thrust loss during landing approach. Though approach is made at partial throttle so that reserve thrust is available from the remaining engines to permit recovery from an engine failure, pilot awareness of the failure through motion cues may not be sufficiently prompt to prevent serious deviations from the nominal path.[2] Studies of the accident potential of these disturbances[3] indicate that longitudinal motion deviations are more dangerous than lateral deviations. The primary effect of wind shear or thrust loss is to change the sink rate of the aircraft, and proper pilot response includes changing the power setting in order to restabilize on the glideslope. Incorrect responses can produce undershoots or overshoots of the runway.

A sink rate increase occurs with a decrease in head wind (i.e., a wind shear). The most severe shear and turbulence conditions appear to arise due to the outflow from thunderstorms and from the passage of warm fronts.[4] The severity of these shear conditions has prompted a number of studies of aircraft response to such disturbances.[3,5-9] The International Civil Aviation Organization and the World Meteorological Organization in 1974 stated an operational requirement for airborne equipment that would enable a pilot to recognize low-level wind shear and turbulence during landing approach and takeoff.[10]

Engine failure on a powered-lift STOL aircraft causes a reduction of total lift and also an asymmetric lift distribution. Thus, the sink rate increases and the aircraft rolls toward the side of the engine loss. Designs for STOL transports, such as the model used in the present study incorporate stability augmentation systems that correct the rolling motion. Also an autospeed loop, using a segment of the lift augmentation flap system as a drag modulator, maintains airspeed. Thus, the increase in sink rate is the primary effect of an engine failure and it must be corrected quickly. Nieuwenhuijse and Franklin[2] describe the results of landing simulations, performed on the NASA Ames Research Center Flight Simulator for Advanced Aircraft, using the STOL transport model, which was also used in the present study. Pilots attempted landings, with engine failures occurring at 100 ft altitude and below, using motion cues and normal piloting techniques. On some runs they detected the failure in sufficient time to respond adequately, but on others they did not. The times required for pilots to respond to the condition were on the order of 1.5 s.

The purpose of the study reported here was to assess whether a state estimator algorithm could be designed to detect a serious wind shear condition or the occurrence of thrust loss more rapidly than a pilot could recognize such conditions from motion cues. The estimator was designed by the technique of quadratic synthesis,[11] utilizing measurements

Presented as Paper 81-0018 at the AIAA 19th Aerospace Sciences Meeting, St. Louis, Mo., Jan. 12-15, 1981; submitted March 2, 1981; revision received Aug. 10, 1981.

*Assistant Professor, Department of Aeronautics and Astronautics FS-10. Member AIAA.

†Professor, Department of Aeronautics and Astronautics. Fellow AIAA.

from various navigation and airdata sensors. It estimates both the motion state of the aircraft and the disturbances being experienced. The output from such an estimator could be fed to the flight control system; however, the present study did not consider the control effects of such a loop closure, but treated the disturbance estimates as alarms that provided a warning to the pilot when threshold levels were exceeded.

The following sections briefly describe the estimator design and present simulation results. The aircraft model used in the study was that of Ref. 2, for which some details are presented in the Appendix. A more extensive discussion of the study and its results are available in Ref. 12.

System Model and Estimator Design

The longitudinal equations of motion for the STOL aircraft of interest were linearized about the nominal approach path described in the Appendix. For a powered-lift STOL aircraft, thrust lag is a significant dynamic characteristic, and a first-order model was used to represent thrust response to commands. The resulting equations have the form:

$$\dot{x}_{ac} = A_{ac}x_{ac} + Bu + Dx_d$$

where the elements of the vectors are:

$$x_{ac} = [uwq\theta c_t]^T \qquad u = [\delta_e \delta_f c_{tc}]^T \qquad x_d = [c_{td} v_{wh} a_h v_{wv} a_v]^T$$

and the values of the matrices are given in the Appendix.

The disturbances of interest (i.e., wind shear and thrust loss) are complex random processes so that any mathematical model of them represents an approximation to the conditions on any given landing. The resulting error in the model used by the estimator can produce biases, and even divergence of the estimates from the actual values. Several authors have discussed this problem,[13-15] and have proposed using Wiener process noise models, which provide integral states to accommodate the biases. Such integral mode models were used in this study as a simple representation of the disturbances (i.e., thrust loss, horizontal and vertical winds, and their rates of change). Thus, the disturbance equations are:

$$\dot{x}_d = A_d x_d + \eta$$

where η contains zero-mean, white noise components and A_d, as given in the Appendix, produces five system poles at $s = 0$.

The sensors assumed in this study were those that would be typical on a large transport aircraft. They included airspeed and angle of attack, pitch rate and angle, ground speed and altitude rate, and acceleration as measured by body-fixed accelerometers. Various combinations of these eight sensors were considered. The linear measurement model for these sensors is given by

$$z = C_{ac}x_{ac} + C_d x_d + \nu$$

where

$$z = [u_a \alpha_a q \theta \dot{h} a_x a_z]^T$$

and ν contains zero-mean, white noise components, and the matrices are given in the Appendix.

The nominal approach flight condition involves unaccelerated motion, so that state estimation by quadratic synthesis can be expected to achieve a steady-state condition with constant gains. Thus, the estimator algorithm has the form:

$$\begin{bmatrix} \dot{\hat{x}}_{ac} \\ \dot{\hat{x}}_d \end{bmatrix} = \begin{bmatrix} A_{ac} & D \\ 0 & A_d \end{bmatrix} \begin{bmatrix} \hat{x}_{ac} \\ \hat{x}_d \end{bmatrix} + \begin{bmatrix} B \\ 0 \end{bmatrix} u + \begin{bmatrix} K_{ac} \\ K_d \end{bmatrix} [z - C_{ac}x_{ac} - C_d x_d]$$

and performance is determined by the choice of the gain matrices K_{ac} and K_d. Gain values could be calculated, using the standard techniques of the steady-state Kalman filter,[11] by selecting spectral density matrices for the noise vectors η and ν. However, the need for rapid response of the estimator and for good damping of its modes (to overcome modeling errors) suggested the use of exponential age-weighting[16,17] in the quadratic cost function of the Kalman filter. This technique is implemented in the calculation of the filter gains by adding a constant α to the diagonal elements of A_{ac} and A_d. The resulting gains are then used with the original estimator algorithm above.

As is known, the Kalman filter provides a stable estimator even for an (observable) unstable system; and when the spectral density of the process noise η is set to zero, the s-plane poles of the estimator are the left half-plane poles of the system plus the reflection in the left half-plane of all right half-plane system poles. The use of age-weighting causes a shift in the origin of the s-plane to the left by α, so that the reflection of poles occurs about $s = -\alpha$. Thus, the combination of age-weighting and zero process noise density in the Kalman filter design permits the predetermined placement of the estimator poles, which is equivalent to selection of the estimator bandwidth.[12] This approach led to a successful estimator design in the present study.

To determine the values of the estimator gains, a measurement noise density matrix must be specified. Since the noise sources are independent, the density matrix has only diagonal elements, each of the form $R_i = 2\tau_m \sigma_i^2$ where σ_i is the rms error in the ith measurement and τ_m is the correlation time of the errors. The values selected here were based on a conservative assessment of the noise characteristics of typical aircraft sensors. The correlation time was taken as $\tau_m = 0.05$ s, and the rms values were those of Table 1.

For the system model defined in the Appendix, the open-loop poles are shown in Fig. 1. The short period and phugoid (which is slightly unstable) are seen, along with the engine response mode at $s = -2.1$, and the five integral modes, which model the disturbances. The locations of these poles and a requirement for a response time of about 1 s in the estimator

Table 1 Measurement noise rms values

$\sigma_{ua} = 1.0$ knot	$\sigma_{\alpha a} = 0.5$ deg	$\sigma_q = 0.5$ deg/s	$\sigma_\theta = 0.5$ deg
$\sigma_{\dot{r}} = 1.7$ ft/s	$\sigma_{\dot{h}} = 1.5$ ft/s	$\sigma_{ax} = 1.6$ ft/s^2	$\sigma_{az} = 1.6$ ft/s^2

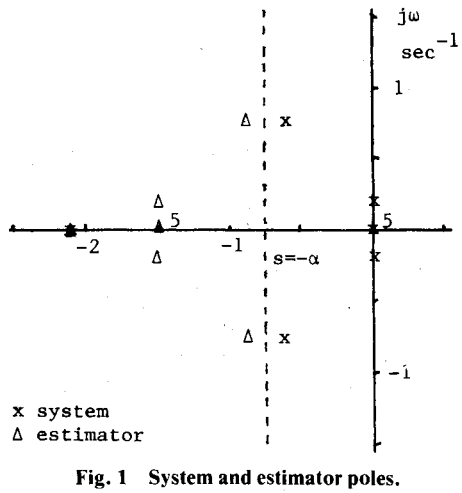

Fig. 1 System and estimator poles.

suggested an age-weighting parameter of $\alpha = 0.75\ s^{-1}$ to provide an appropriate pass band. This value shifted the slower modes to the left, providing the estimator poles shown in Fig. 1. The resulting gains for an eight-measurement case are given in the Appendix.

Performance Evaluation

To verify performance of estimator designs a 3-degree-of-freedom digital simulation of the aircraft longitudinal motions was constructed.[12] The stability augmentation and autospeed loops were included along with input data for pilot commands to thrust lever and column. Two models for the mean wind were included: 1) a logarithmic boundary-layer model for the horizontal wind,[18] and 2) a tabular representation of a thunderstorm outflow.[7] To each, turbulence was added with parameters of standard deviation and scale length provided as inputs.[19] Sensor outputs were generated from the simulated state vector of the system with noise added at the levels indicated in Table 1. Estimator designs were converted to discrete form and implemented in the simulation with a sample rate of 10/s.

The response and cross-coupling characteristics of the estimator design described above were checked using the simulation by providing step inputs to the disturbances while setting the turbulence and measurement noise to zero. Figure 2 shows the effect of a step in c_{td} of 15% of maximum thrust (T_{max}), equivalent to the loss of one engine. The estimate $\hat{c}_t$ responds rapidly and, although some cross coupling into the shear estimates occurs, the amount is not large, and the errors damp well as the error in $\hat{c}_t$ is removed. Similar results were obtained with 1 knot/s step inputs to a_h and a_v. The estimate errors damped within 5 s and thrust disturbance estimate $\hat{c}_{td}$ showed less than a 1% T_{max} excursion.

A more significant test of the estimator is provided by a simulation case that consists of approach from 250 ft altitude in a boundary layer mean wind with severe turbulence and an engine failure at about 200 ft. The wind model provides a headwind of 30 knots at 250 ft, which shears to 15 knots at touchdown, with horizontal and vertical turbulence parameters (i.e., rms and scale length) of[19]

$\sigma_h = 9$ knots $\quad L_h = 250$ ft $\quad \sigma_v = 3$ knots $\quad L_v = 100$ ft

Approach is made at 60% T_{max} but an engine fails after 3 s, reducing thrust by 15% T_{max}. At 6 s, a throttle input is provided (simulating pilot response to the failure), bringing the remaining engines to full thrust, which represents 75% T_{max}. At 12.5 s, a column input is provided (simulating flare), which takes the pitch angle from -3 deg to 8 deg. Touchdown occurs at 17 s. The nominal path about which the state estimates are made is a no-wind path, and the simulated aircraft is trimmed to the initial wind at 250 ft. The actual path drops below the nominal due to wind shear and engine failure, reaching a peak sink rate of 25 ft/s at about 6 s, but the thrust increase and flare produce an acceptable sink rate at touchdown.

Figure 3 shows the disturbance estimates for thrust coefficient $\hat{c}_t$ and horizontal wind $\hat{v}_{wh}$ and shear $\hat{a}_h$, when the eight sensors described above are used. The solid curves in these plots represent actual time histories of disturbances from the simulation, while the points represent the estimates (at 10 samples/s). The thrust estimate is seen to respond to the engine failure within a second of its occurrence; the noise in this estimate was found to be due predominantly to noise in the ground speed measurement.[12] During the same time period, the horizontal wind underwent rapid changes due to the severe level of turbulence present. The wind estimate follows these changes and the shear estimate follows the changes in the rate of the wind with a lag of about 1 s. To indicate a level of severe shear, a threshold value is shown on the plot, and a warning would be provided to the pilot when the shear estimate exceeds this value. The vertical wind did

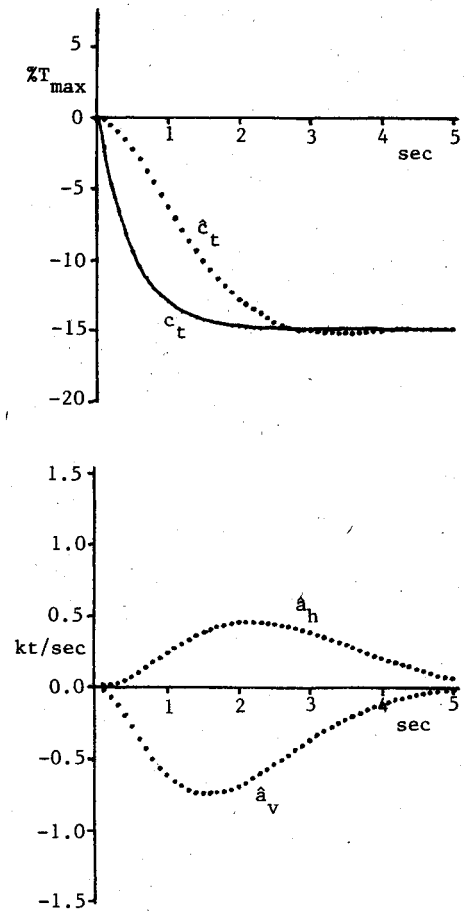

Fig. 2 Response to -15% T_{max} thrust step.

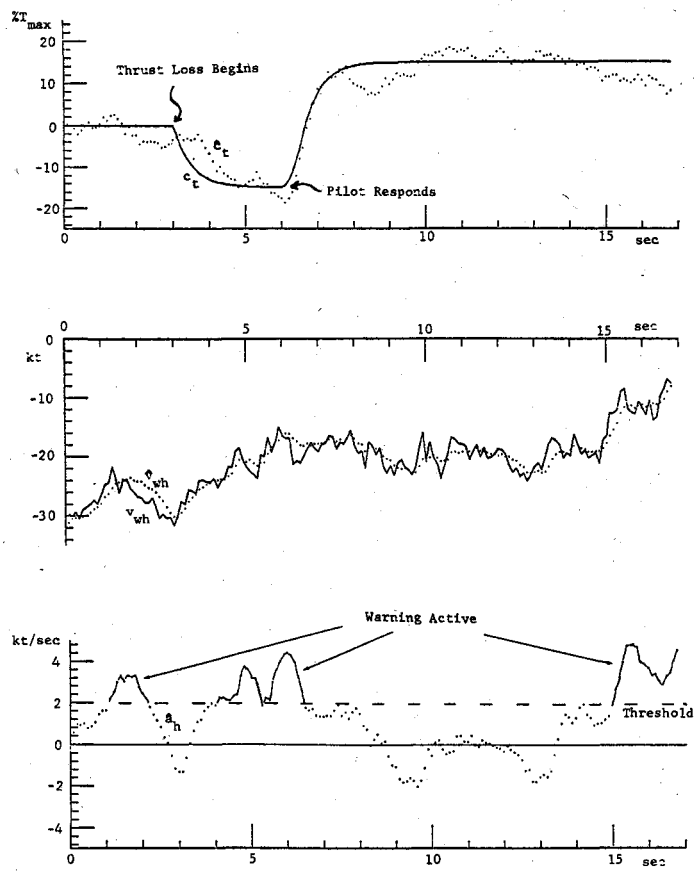

Fig. 3 Estimator response to thrust loss and boundary-layer wind shear with turbulence and random measurement errors.

Table 2 System model

$$A_{ac}=\begin{bmatrix} -0.0064 & 0.118 & -0.0544 & -0.332 & 0.0096 \\ -0.31 & -0.455 & 1.40 & 0.0194 & -0.113 \\ -0.0648 & -0.436 & -0.76 & 0 & -0.055 \\ 0 & 0 & 1 & 0 & 0 \\ 0 & 0 & 0 & 0 & -2.1 \end{bmatrix} \quad B=\begin{bmatrix} 0 & -0.145 & 0 \\ 0 & -0.16 & 0 \\ -1.5 & 0.0607 & 0 \\ 0 & 0 & 0 \\ 0 & 0 & 2.1 \end{bmatrix}$$

$$A_d=\begin{bmatrix} 0 & 0 & 0 & 0 & 0 \\ 0 & 0 & 1 & 0 & 0 \\ 0 & 0 & 0 & 0 & 0 \\ 0 & 0 & 0 & 0 & 1 \\ 0 & 0 & 0 & 0 & 0 \end{bmatrix} \quad D=\begin{bmatrix} 0 & 0.0133 & 0 & 0.117 & 0 \\ 0 & 0.283 & 0 & -0.472 & 0 \\ 0 & 0.0392 & 0 & -0.439 & 0 \\ 0 & 0 & 0 & 0 & 0 \\ 2.1 & 0 & 0 & 0 & 0 \end{bmatrix}$$

Units: knot, deg, s, % T_{max}.

Table 3 Sensor and estimator parameters

$$C_{ac}=\begin{bmatrix} 1 & 0 & 0 & 0 & 0 \\ -0.0278 & 0.715 & 0 & 0 & 0 \\ 0 & 0 & 1 & 0 & 0 \\ 0 & 0 & 0 & 1 & 0 \\ 1.685 & -0.0985 & 0 & 0.229 & 0 \\ -0.0985 & -1.685 & 0 & 2.35 & 0 \\ -0.0108 & 0.199 & 0 & 0 & 0.0162 \\ -0.523 & -0.768 & -0.00454 & 0 & -0.19 \end{bmatrix}$$

$$C_d=\begin{bmatrix} 0 & -0.998 & 0 & 0.0584 & 0 \\ 0 & 0.0695 & 0 & 0.712 & 0 \\ 0 & 0 & 0 & 0 & 0 \\ 0 & 0 & 0 & 0 & 0 \\ 0 & 0 & 0 & 0 & 0 \\ 0 & 0 & 0 & 0 & 0 \\ 0 & 0.0224 & 0 & 0.198 & 0 \\ 0 & 0.4775 & 0 & -0.797 & 0 \end{bmatrix}$$

$$K_{ac}=\begin{bmatrix} -0.0250 & 0.0929 & -0.102 & -0.465 & 0.903 & -0.0374 & 0.0039 & -0.0196 \\ -0.0662 & 0.0958 & 1.241 & 2.840 & -0.150 & -1.155 & -0.0279 & 0.363 \\ 0.0462 & -0.240 & 0.694 & 0.415 & -0.0175 & -0.123 & -0.0195 & 0.167 \\ -0.0172 & -0.0548 & 0.415 & 1.786 & -0.0573 & -0.0601 & -0.0078 & 0.0835 \\ -3.80 & -10.61 & -8.18 & -3.998 & 0.209 & 2.573 & 0.175 & -3.446 \end{bmatrix}$$

$$K_d=\begin{bmatrix} -3.80 & -10.61 & -8.18 & -3.998 & 0.209 & 2.573 & 0.175 & -3.446 \\ -2.589 & 1.321 & -0.378 & -0.566 & 0.926 & -0.0052 & 0.0647 & 0.120 \\ -1.64 & 1.903 & -0.148 & -0.339 & 0.0281 & 0.0705 & 0.0606 & 0.0745 \\ -0.0598 & 2.559 & -1.55 & -2.892 & 0.112 & 1.112 & 0.0744 & -0.310 \\ -0.309 & 0.820 & -1.845 & -1.003 & 0.0478 & 0.426 & 0.0711 & -0.587 \end{bmatrix}$$

Units: as in Tables 1 and 2.

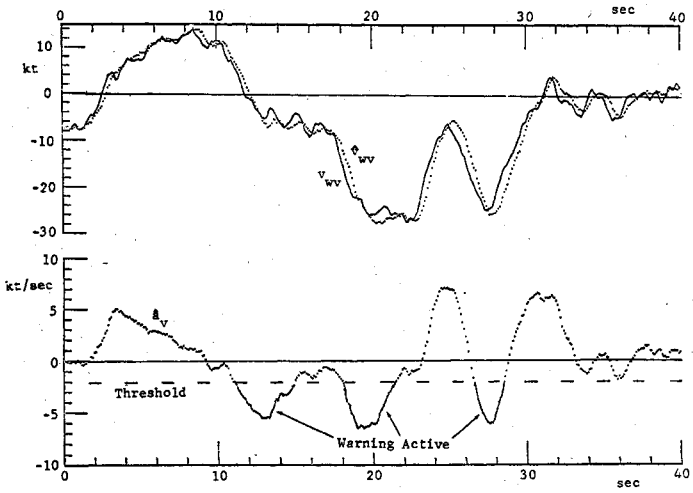

Fig. 4 Estimator response to vertical wind and shear from thunderstorm outflow with turbulence and random measurement errors.

not undergo such severe changes and no shear warnings occurred in that channel. Thus, the estimator design demonstrated its capability to separate these effects and warn of serious conditions when present.

Another case, which was chosen to provide significant vertical wind components, was a path obtained from the thunderstorm model[7] beginning at 900 ft altitude and −9000 ft range. The aircraft was trimmed to the initial wind, consisting of a 5-knot headwind and a 7.6-knot downdraft. No engine failure or pilot inputs were included, so the aircraft simply responded to the wind environment. A peak sink rate of about 50 ft/s occurred at about 23 s, but this reduced to about 20 ft/s at 40 s when touchdown occurred.

Figure 4 shows the vertical wind and shear, which was the most interesting output for this case. Warnings of downdrafts, which would produce high sink rate, clearly follow rapid changes in the wind, though severe variations between 22 s and 30 s cause the estimator to lag. This error shows up in other estimates as well; but when the variations subside, the estimates settle without divergence.

Conclusions

A major purpose of this study was to assess the feasibility of designing a constant-gain estimator that could detect engine failure or severe wind shear more rapidly than can be done by a pilot. The results indicate that useful disturbance estimator designs can be achieved provided that integral modes are included in the dynamic model to accommodate the effects of modeling errors. Also, adequate velocity sensing relative to the Earth (i.e., ground speed and altitude rate) was found to be necessary so that airmass motions can be distinguished from aircraft inertial motions. Further discussion and examples are presented in Ref. 12.

Acknowledgments

This work was supported by Grant NGR 05-020-019 from the NASA Ames Research Center, and thanks are due to Dr. J.A. Franklin for his contributions of data and direction. Thanks are also due to Professor D.B. deBra for his helpful reviews and comments on the study.

Appendix

The aircraft model used in this study was based upon the model in Ref. 2 and is described in Ref. 12. It represents a four-engine, high-wing, medium transport that utilizes externally blown flaps for lift augmentation. The longitudinal controls include thrust command c_{tc}, elevator angle δ_e, and the aft segment of the flap system δ_f, which acts as a drag modulator for speed control. The nominal approach conditions include a speed of 80.2 knots, a flight path angle of −5.57 deg, a pitch angle of −3.35 deg, and a thrust level of 60% T_{max}.

The longitudinal equations of motion have the standard linearized form, as given in the text, and the coefficient matrices for the STOL transport (A_{AC} and B) are shown in Table 2. The disturbance model is also linearized, with engine failure represented by thrust coefficient disturbance, and airmass motions represented by horizontal and vertical winds, and their rates of change. The disturbance coefficient matrices A_d and D are also shown in Table 2.

The deviations of the sensor outputs from nominal are determined from a consideration of the sensor characteristics and their mounting geometry. The measurement coefficient matrices C_{ac} and C_d, for the eight sensors identified in the text, are given in Table 3.

The estimator algorithm is constructed from the models in Tables 2 and 3 and, for the simulated cases reported here, its gain matrices K_{ac} and K_d are given in Table 3.

References

[1] Williamson, G.G., Lewellen, W.S., and Teske, M.E., "Model Predictions of Wind and Turbulence Profiles Associated with an Ensemble of Aircraft Accidents," NASA CR-2884, July 1977.

[2] Nieuwenhuijse, A.W. and Franklin, J.A., "A Simulator Investigation of Engine Failure Compensation for Powered-lift STOL Aircraft," NASA TM Z-62363, May 1974.

[3] Frost, W. and Reddy, K.R., "Investigation of Aircraft Landing in Variable Wind Fields," NASA CR-3073, Dec. 1978.

[4] Skully, R.P., "Low Level Wind Shear," *FAA Advisory Circular 00-50,* April 1976.

[5] Sherman, W.L., "A Theoretical Analysis of Airplane Longitudinal Stability and Control as Affected by Wind Shear," NASA TN D-8596, July 1977.

[6] Bray, R.S., "Factors Influencing Tolerance to Wind Shears in Landing Approach," Paper no. 5 in NASA SP-416, Oct. 1976, pp. 63-76.

[7] Gartner, W.B., "Piloted Flight Simulation Study of Low-Level Wind Shear, Parts 1 and 2," unnumbered interim reports to FAA by SRI International, March and May 1977.

[8] Reid, L.D., Markov, A.B., and Graf, W.O., "The Application of Techniques for Predicting STOL Aircraft Response to Wind Shear and Turbulence During the Landing Approach," University of Toronto Institute for Aerospace Studies, Report No. 215, June 1977.

[9] Hoh, R.H., "Investigation of Vulnerability of Powered-lift STOL to Wind Shear," AIAA Paper No. 77-1120, Atmospheric Flight Mechanics Conference, Hollywood, Fla., Aug. 1977.

[10] Beaulieu, G., "The Effects of Wind Shear on Aircraft Flight Path and Methods of Remote Sensing and Reporting of Wind Shear at Airports," University of Toronto Institute for Aerospace Studies Technical Note No. 216, Feb. 1978.

[11] Bryson, A.E. and Hall, W.E., "Optimal Control and Filter Synthesis by Eigenvector Decomposition," Stanford University Department of Aeronautics and Astronautics, Report No. 436, Dec. 1971.

[12] Bossi, J.A. and Bryson, A.E., "Estimation of Wind Shear and Thrust Loss During STOL Aircraft Landing Approach," Stanford University Department of Aeronautics and Astronautics, Report No. 519, Jan. 1980.

[13] Fitzgerald, R.J., "Divergence in the Kalman Filter," *IEEE Transactions on Automatic Control,* Vol. AC-16, No. 6, Dec. 1971, pp. 736-747.

[14] Athans, M., "The Compensated Kalman Filter," *Proceedings of 2nd Symposium on Nonlinear Estimation Theory and Its Applications,* San Diego, Calif., Sept. 1971, pp. 10-22.

[15] Kwatny, H.G., "Optimal Linear Control Theory and a Class of PI Controllers for Process Control," Paper No. 10-1, *Joint Automatic Control Conference,* Stanford, Calif., 1972, pp. 274-281.

[16] Bryson, A.E., "Kalman Filter Divergence and Aircraft Motion Estimators," *Journal of Guidance and Control,* Vol. 1, Jan. 1978, pp. 71-79.

[17] Anderson, B.D.O., "Exponential Data Weighting in the Kalman-Bucy Filter," *Information Sciences,* Vol. 5, 1973, pp. 217-230.

[18] Luers, J.K., "A Model of Wind Shear and Turbulence in the Surface Boundary Layer," NASA CR-2288, July 1973.

[19] Holley, W.E. and Bryson, A.E., "Wind Modeling and Laternal Aircraft Control for Automatic Landing," Stanford University Department of Aeronautics and Astronautics, Report 489, Jan. 1975.